Factorization method and irregular inclusions in electrical impedance tomography

Bastian Gebauer[1] and Nuutti Hyvönen[2]

[1] Johan Radon Institute for Computational and Applied Mathematics (RICAM), Austrian Academy of Sciences, Altenbergerstr. 69, 4040 Linz, Austria
[2] Institute of Mathematics, Helsinki University of Technology, FI-02015 HUT, Finland

E-mail: `bastian.gebauer@ricam.oeaw.ac.at`, `nuutti.hyvonen@hut.fi`

Abstract. In electrical impedance tomography, one tries to recover the conductivity inside a physical body from boundary measurements of current and voltage. In many practically important situations, the investigated object has known background conductivity but it is contaminated by inhomogeneities. The factorization method of Andreas Kirsch provides a tool for locating such inclusions. Earlier, it has been shown that under suitable regularity conditions positive (or negative) inhomogeneities can be characterized by the factorization technique if the conductivity or one of its higher normal derivatives jumps on the boundaries of the inclusions. In this work, we use a monotonicity argument to generalize these results: We show that the factorization method provides a characterization of an open inclusion (modulo its boundary) if each point inside the inhomogeneity has an open neighbourhood where the perturbation of the conductivity is strictly positive (or negative) definite. In particular, we do not assume any regularity of the inclusion boundary or set any conditions on the behaviour of the perturbed conductivity at the inclusion boundary. Our theoretical findings are verified by two-dimensional numerical experiments.

AMS classification scheme numbers: 35R30, 35Q60, 35J25

1. Introduction

Let us consider the inverse boundary value problem corresponding to *electrical impedance tomography* (EIT): Determine the conductivity tensor $\sigma(x) > 0$ in the elliptic equation

$$\nabla \cdot \sigma \nabla u = 0 \quad \text{in } \Omega$$

when all possible pairs of Neumann and Dirichlet boundary values of the electromagnetic potential u are measured on $\partial\Omega$. This problem was posed by Calderón in 1980 [14] and its unique solvability for isotropic, i.e. scalar, conductivities of a wide class was obtained in three and higher space dimensions by Sylvester and Uhlmann in 1987 [42] and in two dimensions by Nachman in 1996 [34]. Their regularity assumptions on the conductivity and the boundary $\partial\Omega$ have been reduced by several authors since [1, 8, 33, 36, 37]. Recently, considerable progress was made as Astala and Päivärinta solved the isotropic problem in two dimensions under the natural regularity $\sigma \in L^\infty(\Omega)$ [4]. On the other hand, it is well known that the inverse problem of EIT is not uniquely solvable without the isotropy assumption (see, e.g., [40]).

The reconstruction methods of EIT can be divided into two categories: iterative and direct algorithms. An iterative method produces a sequence of approximations for the unknown conductivity. The iteration is finished when some beforehand chosen stopping criterion is satisfied. In most cases, the used optimization procedure is based on the output least squares formulation of the inverse problem and on some regularized Newton-type algorithm. The most fundamental of the direct reconstruction algorithms is the one by Siltanen, Mueller and Isaacson [38] since it is a numerical implementation of Nachman's constructive uniqueness proof in two dimensions [34]. Other direct methods include the layer stripping algorithm [39, 41], the factorization method [10, 11, 29] and the probe method [28] together with their variants. For more details on the reconstruction algorithms, we refer to the review articles [6, 15] and the references therein.

Various practically important imaging problems consider locating inhomogeneities inside objects with known background conductivities. For example, detection of cracks and air bubbles in some building material and distinguishing cancerous tissue from healthy background fall into this category of problems. The factorization method, introduced within inverse obstacle scattering by Kirsch [29] and modified to the framework of EIT by Brühl and Hanke [9, 10, 11], provides a tool that can be applied to these kinds of situations. When the factorization method is considered within EIT, its functionality can be secured by assuming that the inclusions are either more or less conductive than the background and the conductivity or one of its higher normal derivatives jumps on the boundaries of the inclusions, cf. [9, 10, 11, 17, 20, 25, 30], and the preprint of Nachman, Päivärinta and Teirilä [35]. However, some inhomogeneities may affect different normal derivatives on different parts of their boundaries or the perturbed conductivity can be altogether smooth, in which case earlier results do not tell if the factorization method works or not. In addition, previous works assume that

the inclusion boundaries are at least Lipschitz continuous.

In this work, we merely assume that the union of the inclusions is an open set with connected complement and the corresponding L^∞-perturbation of the conductivity is positive (or negative) semidefinite. We show that the factorization method finds every point of the inhomogeneity that has an open neighbourhood where the perturbation is strictly positive (or negative). Notice that the size of the neighbourhood and the lower bound for the conductivity may depend on the considered point and we do not pose any regularity on the inclusion boundary. Inhomogeneities where every interior point has such a neighbourhood are herein called *locally strictly positive* (or *negative*). This kind of irregular inclusions can be characterized via boundary measurements in the manner described originally in [9], with the slight drawback that the outcome of the range test is uncertain if the probe location is exactly on the boundary of the inhomogeneity. In particular, note that we do not set any conditions on the behaviour of the perturbed conductivity at the inclusion boundary.

This text is organized as follows. In section 2, we state and prove our characterization result. Section 3 presents the numerical experiments and section 4 contains concluding remarks.

2. Characterization of an irregular inclusion

Let $\Omega \subset \mathbb{R}^n$, $n \geq 2$, be a smooth domain and $\sigma : \Omega \to \mathbb{R}^{n \times n}$ the corresponding symmetric conductivity tensor. The static forward problem of EIT is as follows: For the input current $f \in L^2_\diamond(\partial\Omega)$, find the electromagnetic potential $u \in H^1(\Omega)/\mathbb{R}$ that is the weak solution of

$$\nabla \cdot \sigma \nabla u = 0 \qquad \text{in } \Omega, \qquad \nu \cdot \sigma \nabla u = f \qquad \text{on } \partial\Omega, \tag{2.1}$$

where ν is the exterior unit normal on $\partial\Omega$ and

$$L^2_\diamond(\partial\Omega) = \left\{ v \in L^2(\partial\Omega) \ \Big| \ \int_{\partial\Omega} v \, \mathrm{d}S = 0 \right\}.$$

If the conductivity $\sigma \in L^\infty(\Omega, \mathbb{R}^{n \times n})$ satisfies the estimate

$$0 < cI \leq \sigma, \qquad c \in \mathbb{R}_+, \tag{2.2}$$

the forward problem (2.1) has a unique solution that depends continuously on the input current. Here and in the following, we use "$<$" in the sense of positive definiteness almost everywhere in Ω.

When solving the inverse problem of EIT, one tries to reconstruct the conductivity σ from the knowledge of the Neumann-to-Dirichlet, or current-to-voltage, map

$$\Lambda_\sigma : f \mapsto u|_{\partial\Omega}, \qquad L^2_\diamond(\partial\Omega) \to L^2(\partial\Omega)/\mathbb{R}.$$

The use of the quotient spaces above emphasizes the freedom to choose the ground level of the potential as one wishes. For our purposes, it is convenient to fix the ground level so that the Dirichlet boundary value of the solution to (2.1) is interpreted as an element of $L^2_\diamond(\partial\Omega)$, which corresponds to identifying $L^2_\diamond(\partial\Omega)$ with its dual space $L^2(\partial\Omega)/\mathbb{R}$. With this convention, Λ_σ is a linear, bounded and self-adjoint map from $L^2_\diamond(\partial\Omega)$ to itself.

2.1. The main result

In this work, we assume that the conductivity inside Ω is of the form

$$\sigma = \begin{cases} I + \kappa & \text{in } D, \\ I & \text{in } \Omega \setminus \overline{D}, \end{cases} \tag{2.3}$$

where D is open, $\overline{D} \subset \Omega$ and $\Omega \setminus \overline{D}$ is connected. Furthermore, the symmetric perturbation $\kappa \in L^\infty(D, \mathbb{R}^{n \times n})$ is assumed to be such that σ satisfies (2.2). Take note that the results presented below would remain valid if the unit conductivity in (2.3) was replaced by any other a priori known background conductivity that satisfies (2.2) and enables unique continuation of Cauchy data from $\partial\Omega$ to the interior of Ω. The same comment applies to the smoothness of the boundary $\partial\Omega$, as well. For example, in the preprint [35] it is assumed that the background conductivity and the boundary $\partial\Omega$ are of Lipschitz class.

In what follows, we will denote the Neumann-to-Dirichlet boundary map corresponding to the perturbed conductivity σ by Λ and the map corresponding to the unit background conductivity by Λ_0. Our goal is to locate the inclusion D via boundary measurements, under only mild conditions on the perturbation κ, by extracting information from the range of the square root of $|\Lambda_0 - \Lambda|$ in a constructive manner. Notice that in real life $|\Lambda_0 - \Lambda|$ can be approximated through electrode measurements, cf. [22] and the preprint [32]. The techniques applied here stem from [29] and they have been used in the framework of inverse elliptic boundary value problems in [2, 5, 9, 10, 11, 12, 13, 16, 17, 20, 21, 22, 23, 24, 25, 26, 27, 30] and the preprints [19, 32, 35], as well.

We first introduce a singular solution for scanning the object Ω. Fix $y \in \Omega$, let $\hat{\alpha} \in \mathbb{R}^n$ be an arbitrary unit vector, and consider the solution Φ_y of the following homogeneous Neumann problem

$$\Delta\Phi(x) = \hat{\alpha} \cdot \nabla_x \delta(x - y) \qquad \text{in } \Omega, \qquad \frac{\partial\Phi}{\partial\nu} = 0 \qquad \text{on } \partial\Omega,$$

where δ is the delta functional and the ground level of the potential is chosen so that $\int_{\partial\Omega} \Phi_y \mathrm{d}S = 0$. Physically, Φ_y corresponds to the electrostatic potential created by a dipole source at y pointing in the direction $\hat{\alpha}$.

We can now state our main result.

Theorem 2.1. *Assume that either $\kappa \geq 0$ or $\kappa \leq 0$. If $y \in D$ has a neighbourhood $U \subset D$ such that $\operatorname{ess\,inf} |\kappa|_U| > 0$, then the boundary potential $\Phi_y|_{\partial\Omega}$ belongs to the range of $|\Lambda_0 - \Lambda|^{1/2}$. Conversely, the boundary potential $\Phi_y|_{\partial\Omega}$ is not included in the range of $|\Lambda_0 - \Lambda|^{1/2}$ if $y \in \Omega \setminus \overline{D}$.*

In many applications, the assumption of the first part of Theorem 2.1 is fulfilled for every point in D. We say that the inclusion D (or the perturbation κ) is locally strictly positive if for each $y \in D$ there exist scalar constants $\epsilon_y, r_y > 0$ such that

$$\kappa > \epsilon_y I \qquad \text{almost everywhere in } B(y, r_y) \subset D, \tag{2.4}$$

where $B(y, r_y)$ denotes the open ball of radius r_y centered at y. Similarly, the inclusion D is called locally strictly negative if κ satisfies (2.4) with $\kappa > \epsilon_y I$ replaced by $\kappa < -\epsilon_y I$. Notice that a locally strictly positive (or locally strictly negative) perturbation may have vanishing traces on ∂D or on some subsets of ∂D. In particular, the resulting perturbed conductivity σ may be smooth in a neighbourhood of ∂D.

Corollary 2.2. *Assume that the inhomogeneity D is either locally strictly positive or locally strictly negative. If $y \in D$, the boundary potential $\Phi_y|_{\partial\Omega}$ belongs to the range of $|\Lambda_0 - \Lambda|^{1/2}$. Conversely, the boundary potential $\Phi_y|_{\partial\Omega}$ is not included in the range of $|\Lambda_0 - \Lambda|^{1/2}$ if $y \in \Omega \setminus \overline{D}$.*

Unlike the results presented in [11, 17, 25, 30] and the preprint [35], this corollary does not tell that $\Phi_y|_{\partial\Omega} \notin |\Lambda_0 - \Lambda|^{1/2}$ when $y \in \partial D$. However, from the practical point of view, our explicit characterization is as good as the ones presented in earlier work.

On the positive side, our assumptions on the inclusion D and the perturbation κ are much weaker than in previous articles on the factorization method within diffuse tomography. Thus far, the weakest regularity assumption on the inclusion boundary has been used in the preprint [35], where D is Lipschitz, but only perfectly conducting inhomogeneities are considered. The theoretical articles dealing with penetrable inclusions have been based on the assumption that D has at least C^2-boundary (cf., e.g., [30]), although in [10] it is noted that the method also works with Lipschitz inhomogeneities. In this work, D is just open. Moreover, the only article that has so far tackled perturbations that are not uniformly strictly positive (or negative) in D, namely [25], assumes that ∂D and $\kappa > 0$ are smooth and all conductivities are isotropic. Furthermore, in [25] the way that κ is allowed to behave on ∂D is quite specific: For some $m \geq 1$, the conductivity and its $m-1$ lowest normal derivatives are assumed to be continuous over the inclusion boundary whereas the mth normal derivative is assumed to jump everywhere on ∂D. In this work, different normal derivatives of the conductivity may jump on different parts of ∂D or the conductivity can be altogether smooth as the L^∞-perturbation κ is only assumed to be locally strictly positive (or negative).

2.2. Proof of the main result

Apart from some considerations in the original article by Brühl [11], the characterization results obtained through the factorization technique within diffuse tomography methods have been based on a factorization of the type (see, e.g., [17])

$$\Lambda_0 - \Lambda = LFL^*,$$

where the last operator L depends on the shape of D, not on the properties inside D. By showing that the intermediate operator F is an 'almost coercive' (cf. [30]) isomorphism between suitable dual Sobolev spaces, one has been able to prove that the range of $|\Lambda_0 - \Lambda|^{1/2}$ coincides with the range of L (cf. [17, 25, 30]). Finally, the actual characterization results have followed from the special structure of L together with the principle of unique continuation.

In this work, we take a different approach. The idea is to extend the already known characterization results to more irregular surroundings by using certain monotonicity properties of the range of $|\Lambda_0 - \Lambda|^{1/2}$. It should be noted that similar arguments were used already in [9, 11]. We begin with a simple well known lemma. Physically speaking, it states that the power needed when applying a boundary current pattern is decreasing with respect to the conductivity.

Lemma 2.3. *Let Λ_1 and Λ_2 be the Neumann-to-Dirichlet maps corresponding to the symmetric conductivities $\sigma_1, \sigma_2 \in L^\infty(\Omega, \mathbb{R}^{n\times n})$, respectively. Assume that σ_1 and σ_2 satisfy (2.2) and $\sigma_1 \leq \sigma_2$. Then it holds that*

$$\langle f, (\Lambda_1 - \Lambda_2)f \rangle_{L^2(\partial\Omega)} \geq 0$$

for any current $f \in L^2_\diamond(\partial\Omega)$.

Proof. The proof for isotropic conductivities can be found, for example, in [11]. The generalization to the anisotropic case follows by using a similar line of reasoning. $\square$

We note that Lemma 2.3 yields, in particular, that the absolute value of the difference of the Neumann-to-Dirichlet maps in Theorem 2.1 is simply the difference itself (for $\kappa \geq 0$) or minus the difference (for $\kappa \leq 0$).

Next we will transform the above monotonicity result into a form that considers ranges of square roots. A similar consideration can be found in [11]. Notice that all square root operators below are obtained by treating the original maps as positive and self-adjoint operators from $L^2_\diamond(\partial\Omega)$ to itself and taking the unique positive and self-adjoint square root.

Lemma 2.4. *Assume that $\sigma_1 \leq \sigma_2$ are as in Lemma 2.3 and let $\sigma_0 \in L^\infty(\Omega, \mathbb{R}^{n\times n})$ be yet another symmetric conductivity that satisfies (2.2). If $\sigma_0 \leq \sigma_1$,*

$$\mathcal{R}\left\{(\Lambda_0 - \Lambda_1)^{1/2}\right\} \subseteq \mathcal{R}\left\{(\Lambda_0 - \Lambda_2)^{1/2}\right\}.$$

Conversely, if $\sigma_2 \leq \sigma_0$, it holds that

$$\mathcal{R}\left\{(\Lambda_2 - \Lambda_0)^{1/2}\right\} \subseteq \mathcal{R}\left\{(\Lambda_1 - \Lambda_0)^{1/2}\right\}.$$

Proof. A functional analytic lemma that is frequently used for the factorization method is that for any continuous linear operator $A : H_1 \to H_2$, between Hilbert spaces H_1 and H_2,

$$y \in R(A) \quad \text{if and only if} \quad \exists C > 0 : \ \langle y, x \rangle_{H_2} \leq C \|A^*x\|_{H_1} \quad \forall x \in H_2.$$

In a Banach space formulation, this is called the "14th important property of Banach spaces" in [7], cf. e. g. [16, Lemma 3.4] for an elementary proof. An immediate consequence is that for self-adjoint operators $A, B : H_1 \to H_1$ the existence of a constant $C > 0$ that satisfies

$$\|Ax\| \leq C \|Bx\|, \qquad \text{for all } x \in H_1,$$

implies that $\mathcal{R}(A) \subseteq \mathcal{R}(B)$.

Let $\sigma_0 \leq \sigma_1 \leq \sigma_2$. From Lemma 2.3 we know that for all $f \in L^2_\diamond(\partial\Omega)$

$$\langle f, (\Lambda_0 - \Lambda_1)f \rangle_{L^2(\partial\Omega)} = \langle f, (\Lambda_0 - \Lambda_2)f \rangle_{L^2(\partial\Omega)} - \langle f, (\Lambda_1 - \Lambda_2)f \rangle_{L^2(\partial\Omega)}$$
$$\leq \langle f, (\Lambda_0 - \Lambda_2)f \rangle_{L^2(\partial\Omega)},$$

meaning that $\left\|(\Lambda_0 - \Lambda_1)^{1/2}f\right\| \leq \left\|(\Lambda_0 - \Lambda_2)^{1/2}f\right\|$ and, thus,

$$\mathcal{R}\left\{(\Lambda_0 - \Lambda_1)^{1/2}\right\} \subseteq \mathcal{R}\left\{(\Lambda_0 - \Lambda_2)^{1/2}\right\}.$$

Since the second part of the assertion follows from the same line of reasoning, the proof is complete. □

Before we can formulate the proof of Theorem 2.1, we still need a characterization result that can be extended using lemma 2.4. We choose a simplified version of the original theorem presented in [11].

Lemma 2.5. *Suppose that the conditions and notations of Theorem 2.1 are valid. In addition, assume that D is connected and has a smooth boundary, and the corresponding perturbation is given as $\kappa = \delta I$, where $\delta \neq 0$ is a constant. Then $\Phi_y|_{\partial\Omega}$ belongs to the range of $|\Lambda_0 - \Lambda|^{1/2}$ if and only if $y \in D$.*

By combining the three lemmas above, we are now ready to present the proof of Theorem 2.1.

Proof of Theorem 2.1. To begin with, assume that $\kappa \geq 0$. If $y \in D$ has a neighbourhood $U \subset D$ such that ess inf $|\kappa|_U| > 0$, there exist scalars $\epsilon_y, r_y > 0$ such that $\kappa > \epsilon_y I$ almost everywhere in $B(y, r_y) \subset U$. We define an auxiliary conductivity tensor by

$$\sigma_y = \begin{cases} I + \epsilon_y I & \text{in } B(y, r_y), \\ I & \text{in } \Omega \setminus \overline{B(y, r_y)}, \end{cases}$$

and denote the associated Neumann-to-Dirichlet map by Λ_y. Due to Lemma 2.5, we see straight away that $\Phi_y|_{\partial\Omega} \in \mathcal{R}\{(\Lambda_0 - \Lambda_y)^{1/2}\}$. Furthermore, since $\sigma_y < \sigma$, it follows from the first part of Lemma 2.4 that also

$$\Phi_y|_{\partial\Omega} \in \mathcal{R}\left\{(\Lambda_0 - \Lambda)^{1/2}\right\} = \mathcal{R}\left\{|\Lambda_0 - \Lambda|^{1/2}\right\},$$

which proves the first part of the claim.

Continue assuming that $\kappa \geq 0$ and let now $y \in \Omega \setminus \overline{D}$. Since $\Omega \setminus \overline{D}$ is open and connected, there exists a connected open set D_y such that $y \notin D_y$, $D \subset D_y$, $\Omega \setminus \overline{D}_y$ is connected and the boundary ∂D_y is smooth. We redefine the auxiliary conductivity by

$$\sigma_y = \begin{cases} I + kI & \text{in } D_y, \\ I & \text{in } \Omega \setminus \overline{D}_y, \end{cases}$$

where the scalar constant $k > 0$ is chosen so that $\sigma_y > \sigma$ almost everywhere in Ω. Now the first part of Lemma 2.4 and Lemma 2.5 tell us that

$$\Phi_y|_{\partial\Omega} \notin \mathcal{R}\left\{(\Lambda_0 - \Lambda_y)^{1/2}\right\} \supseteq \mathcal{R}\left\{(\Lambda_0 - \Lambda)^{1/2}\right\} = \mathcal{R}\left\{|\Lambda_0 - \Lambda|^{1/2}\right\},$$

where Λ_y is once again the Neumann-to-Dirichlet map corresponding to σ_y. This proves the claim for $\kappa \geq 0$.

The case that $\kappa \leq 0$ can be handled in the same way, with the exception that this time one uses the second part of Lemma 2.4 instead of the first part. This completes the proof. $\square$

3. Numerical experiments

To verify our theoretical findings, we consider three test examples that are not covered by previous works on the factorization method. In all three cases, Ω is the two-dimensional unit disk and on $\partial\Omega$ we apply the L^2-orthonormal basis functions

$$\left\{ \frac{1}{\sqrt{\pi}}\sin(n\phi),\ \frac{1}{\sqrt{\pi}}\cos(n\phi)\ \Big|\ n = 1,\ldots,128 \right\}$$

as input currents. Here and in the following, the pair (r,ϕ) denotes the polar coordinates with respect to the center of Ω. We denote the potentials corresponding to the perturbed conductivity (2.3) and the unit background conductivity by u and u_0, respectively, and use the commercial finite element software Comsol to compute the difference $v := u_0 - u \in H^1(\Omega)/\mathbb{R}$ by solving the variational problem

$$\int_\Omega \sigma \nabla v \cdot \nabla w \, \mathrm{d}x = \int_D \kappa \nabla u_0 \cdot \nabla w \, \mathrm{d}x \qquad \text{for all } w \in H^1(\Omega), \tag{3.1}$$

which is obtained by subtracting the variational equations for u and u_0. Since $(\sigma - I)$ vanishes in a neighbourhood of $\partial\Omega$, (3.1) is equivalent to

$$\nabla \cdot \sigma \nabla v = \nabla \cdot (\sigma - I)\nabla u_0$$

with homogeneous Neumann boundary condition on $\partial\Omega$. On the right hand side we use the exact solution

$$u_0 = \frac{1}{n\sqrt{\pi}}\sin(n\phi)r^n, \quad \text{resp.,} \quad u_0 = \frac{1}{n\sqrt{\pi}}\cos(n\phi)r^n.$$

As the difference of u and u_0 is considerably smaller than u and u_0, this approach leads to a higher precision than computing u and u_0 separately. The boundary data $v|_{\partial\Omega} = (u_0 - u)|_{\partial\Omega}$ is then expanded in the aforementioned trigonometric basis, which gives a discrete approximation $M \in \mathbb{R}^{256 \times 256}$ of the operator $\Lambda_0 - \Lambda$.

Recall that Corollary 2.2 yields a binary criterion to decide whether a point lies inside the inclusion D or not, i.e., for every $y \notin \partial D$

$$\Phi_y|_{\partial\Omega} \in \mathcal{R}(|\Lambda_0 - \Lambda|^{1/2}) \quad \Longleftrightarrow \quad y \in D.$$

For the numerical implementation of this range test, we follow [18]. Let

$$(\Lambda_0 - \Lambda)v_k = \lambda_k v_k, \qquad k \in \mathbb{N},$$

be the spectral decomposition of the compact, self-adjoint, and injective operator $\Lambda_0 - \Lambda$ with orthonormal basis of eigenfunctions $\{v_k\} \subset L^2_\diamond(\partial\Omega)$ and eigenvalues $\{\lambda_k\} \subset \mathbb{R}$ (sorted in decreasing order of absolute value). The Picard criterion yields that

$$\Phi_y|_{\partial\Omega} \in \mathcal{R}(|\Lambda_0 - \Lambda|^{1/2})$$

if and only if

$$f(y) := \frac{1}{\|\Phi_y|_{\partial\Omega}\|^2_{L^2(\partial\Omega)}} \sum_{k=1}^{\infty} \frac{|\langle \Phi_y|_{\partial\Omega}, v_k \rangle_{L^2(\partial\Omega)}|^2}{|\lambda_k|} < \infty.$$

Using a singular value decomposition of the discrete approximation $M \in \mathbb{R}^{256 \times 256}$

$$M\tilde{v}_k = \tilde{\lambda}_k \tilde{u}_k, \qquad M^* \tilde{u}_k = \tilde{\lambda}_k \tilde{v}_k, \qquad k = 1, \dots, 256,$$

with nonnegative $\{\tilde{\lambda}_k\} \subset \mathbb{R}$ (sorted in decreasing order) and orthonormal bases $\{\tilde{u}_k\}, \{\tilde{v}_k\} \subset \mathbb{R}^{256}$, we approximate the function $f(y)$ by

$$\tilde{f}(y) := \sum_{k=1}^{m} \frac{(\tilde{\Phi}_y \cdot \tilde{v}_k)^2}{|\tilde{\lambda}_k|} \Big/ \sum_{k=1}^{m} (\tilde{\Phi}_y \cdot \tilde{v}_k)^2,$$

where $\tilde{\Phi}_y \in \mathbb{R}^{256}$ contains the Fourier coefficients of $\Phi_y|_{\partial\Omega}$ and m is chosen so that $\tilde{\lambda}_{m+1}$ is the first singular value below the expected measurement error. For a theoretical study of the connection between the infinite Picard series for the Neumann-to-Dirichlet map $\Lambda_0 - \Lambda$ and the truncated Picard series for its finite-dimensional approximation M, we refer the reader to a recent work of Lechleiter [31].

To obtain a numerical criterion telling whether a point y belongs to the unknown inclusion D or not, one has to decide if the infinite sum $f(y)$ attains the value ∞ by using the approximate value $\tilde{f}(y)$, which is always finite. Thus, a threshold $\tilde{C}_\infty > 0$ is needed to distinguish points with *large* values $\tilde{f}(y) \geq \tilde{C}_\infty$ from those with *small* values $\tilde{f}(y) < \tilde{C}_\infty$. A reconstruction of D is then obtained by evaluating $\tilde{f}(y)$ on a grid of points $\{y_n\} \subset \Omega$ and saying that all points with $\tilde{f}(y_n) < \tilde{C}_\infty$ belong to the inclusion. Choosing different threshold values $\tilde{C}_\infty$ corresponds to choosing different level contours of $\tilde{f}(y)$ or, equivalently, of a monotone function of $\tilde{f}(y)$.

In our numerical experiments, we plot the indicator function

$$\text{Ind}(y) := \left(\log \tilde{f}(y) \right)^{-1} \tag{3.2}$$

on an equidistant grid $\{y_n\} \subset \Omega$, which is chosen independently of the finite element mesh that is used for solving the forward problems. We also show the largest level contour that is still inside the true inclusion D, i.e., the one corresponding to the threshold value

$$\hat{C}_\infty := \inf \left\{ C_\infty \in \mathbb{R} \ \middle|\ \text{Ind}^{-1}(]C_\infty, \infty[) \subseteq D \right\}.$$

In our numerical experiments we obtained $\hat{C}_\infty$ by comparing the level contours to the true inclusion D. In practice, the choice of the threshold requires additional information, e.g., from previous experiments, and there is no guarantee that an optimal contour is found. To illustrate the sensitivity of our reconstructions with respect to the threshold, we also plot the level contours $\text{Ind}^{-1}(C_\infty)$ for $C_\infty = 0.9 \cdot \hat{C}_\infty$ and $C_\infty = 1.1 \cdot \hat{C}_\infty$.

Figure 1 shows the exact conductivities σ for the three test examples. In the first example, the inclusion D is a disk of radius $R = 0.3$ and the perturbation κ is given by $\exp(R^{-1} - (R^2 - \rho^2)^{-1/2})$, where ρ is the distance from the center of D. Notice that this results in a smooth σ with maximal value 2. In the second example, the object Ω is
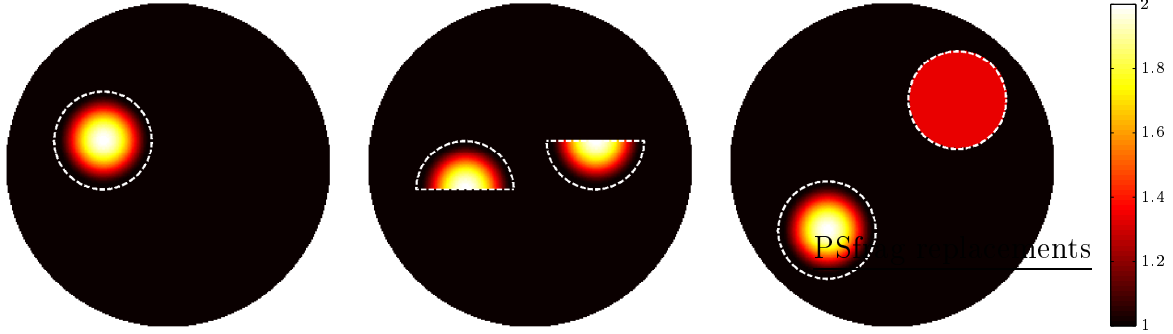
Figure 1. Exact conductivities for the three test cases.
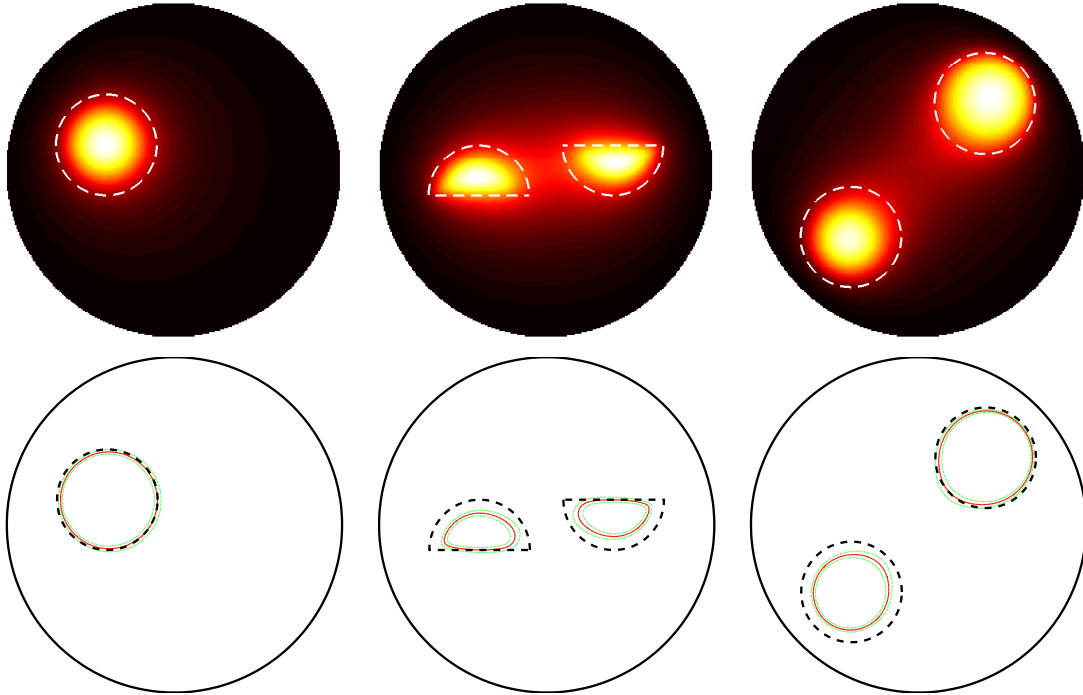
Figure 2. Numerical reconstructions for exact simulated data.

contaminated by two inhomogeneities that are constructed by multiplying the smooth perturbation introduced in the first test by the characteristic function of a semidisk to obtain inclusions with a jump of conductivity on one side and a smooth transition on the other side. In the last test, we use the smooth inclusion of the first experiment together with an inhomogeneity where the conductivity jumps by a constant value. The boundaries of the inclusions, i.e. of the supports of the perturbations, are plotted by dashed white line.

Figure 2 illustrates the reconstructions that we obtained using exact simulated data. The first row shows the graph of the indicator function Ind, defined by (3.2), for the three tests and the second row shows the corresponding level curves for the threshold $\hat{C}_\infty$ (solid line), that is optimal in the sense explained above, and for the two perturbed

thresholds $0.9 \cdot \hat{C}_\infty$ (outer dotted line) and $1.1 \cdot \hat{C}_\infty$ (inner dotted line). The true inclusions are once again marked with a dashed line. As Figure 2 demonstrates, all inclusions were found in all three tests. Although the gradient of the indicator Ind is a little bit steeper over the parts of the inclusion boundary where the perturbed conductivity jumps than over those parts where the transition is smooth, the quality of the reconstructions does not seem to depend very much on the behaviour of the perturbed conductivity at the inclusion boundary.

Since one might be tempted to compare the first row of Figure 2 directly with the exact conductivities in Figure 1, let us stress that the factorization method is designed only to reconstruct the support of the unknown perturbation but not the perturbation itself. The indicator function Ind attains much larger values inside the inclusion D than on its outside; however, we have no theoretical evidence that these values can be directly related to the actual perturbed conductivity. In fact, the second and the third example suggest that the behaviour of Ind depends mainly on the distance to the inclusion boundary ∂D, cf. also the work of Arens [3] for theoretical results of such a dependence in the context of inverse scattering.

In addition to using the unperturbed simulated measurement matrix M, we also test the method after adding 0.1% noise to M. More precisely, we generate a random matrix $E \in \mathbb{R}^{256 \times 256}$ with uniformly distributed entries between -1 and 1. Then E is scaled to the noise level with respect to its spectral norm $\|E\|_2$ and added to M, i.e., we replace M with

$$M_\epsilon := M + 10^{-3} \|M\|_2 \frac{E}{\|E\|_2}.$$

Accordingly, only singular values larger than $10^{-3} \|M_\epsilon\|$ are now used in the truncated Picard series in the definition of $\tilde{f}(y)$.

Figure 3, which is organized in the same way as Figure 2, illustrates the reconstructions corresponding to our three test cases with noisy simulated data. As one might expect, the graphs of the indicator function Ind shown on the first row of Figure 3 are more blurred than the corresponding ones in the noiseless case. In addition, the level curves of Ind, plotted on the second row, do not capture the shapes of the inclusions very well and it seems that the quality of the obtained reconstructions is rather sensitive to the choice of the threshold. Anyway, with this relatively low noise level, the reconstructions still contain information on the size, location and number of the inclusions. For more detailed studies on the effect of noise on the general performance of the factorization method, we refer the reader to the works cited in our introduction.

All above examples confirm our theoretical result: The factorization method does not rely on a jump in the conductivity but merely on the fact that the conductivity at each point inside the inclusion is higher (or lower) than the conductivity of the background medium.
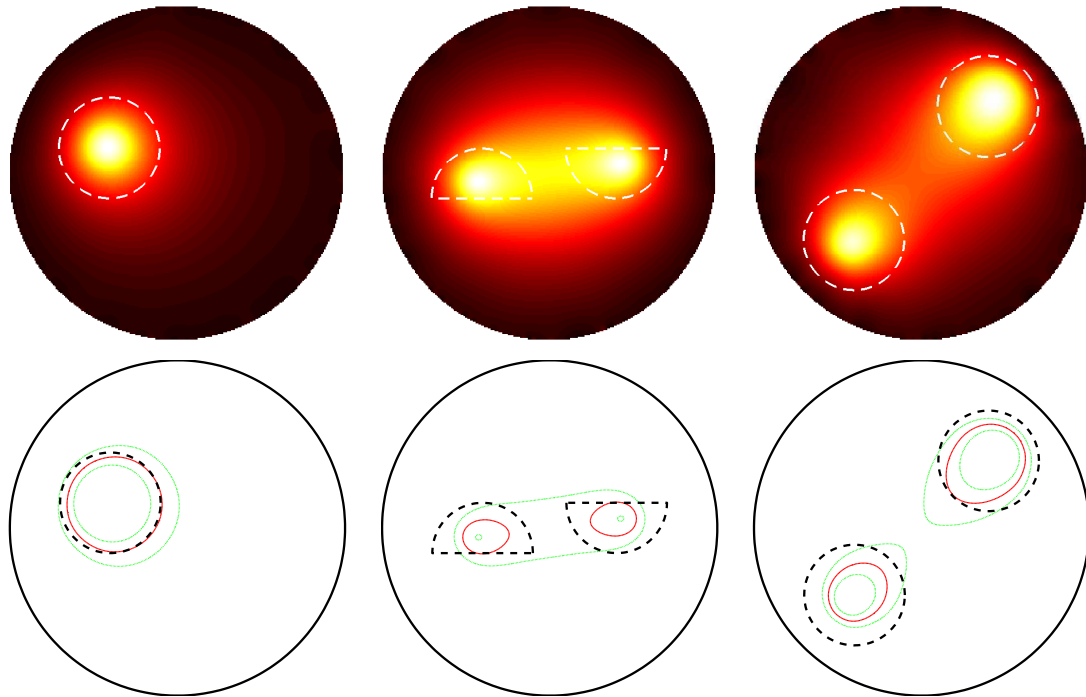
Figure 3. Numerical reconstructions for noisy data.

4. Conclusions

We have shown that in EIT the factorization method works even if the inclusions have no boundary regularity and there is no sharp jump in the conductivity or in one of its higher derivatives on the inclusion boundary. Numerical examples with simulated data confirm our theoretical results.

Our analysis is based on a monotonicity argument which allows us to generalize previously known results on the factorization method. Although we restricted our attention to EIT, the same arguments hold when applying the factorization method to other real elliptic inverse boundary value problems (cf. [17]) like optical tomography or elasticity measurements. We also expect that similar results can be obtained in inverse obstacle scattering.

Acknowledgments

References

[1] Alessandrini G 1990 Singular solutions of elliptic equations and the determination of conductivity by boundary measurements *J. Differential Equations* **84** 252–72

[2] Ammari H, Griesmaier R and Hanke M 2007 Identification of small inhomogeneities: asymptotic factorization *Math. Comp.* **76** 1425–48

[3] Arens T 2004 Why linear sampling works *Inverse Problems* **20** 163–73

[4] Astala K and Päivärinta L 2006 Calderón's inverse conductivity problem in the plane *Ann. of Math.* **163** 265–99

[5] Bal G 2005 Reconstructions in impedance and optical tomography with singular interfaces *Inverse Problems* **21** 113–31

[6] Borcea L 2002 Electrical impedance tomography *Inverse Problems* **18** R99–R136

[7] Bourbaki N 2003 *Topological Vector Spaces, Chapters 1–5*, Elem. Math. (Berlin:Springer-Verlag)

[8] Brown R M and Uhlmann G 1997 Uniqueness in the inverse conductivity problem for non-smooth conductivities in two dimensions *Comm. Partial Differential Equations* **22** 1009–27

[9] Brühl M 1999 Gebietserkennung in der elektrischen Impedanztomographie *Dissertation* Universität Karlsruhe

[10] Brühl M and Hanke M 2000 Numerical implementation of two noniterative methods for locating inclusions by impedance tomography *Inverse Problems* **16** 1029–42

[11] Brühl M 2001 Explicit characterization of inclusions in electrical impedance tomography *SIAM J. Math. Anal.* **32** 1327–41

[12] Brühl M, Hanke M and Pidcock M 2001 Crack detection using electrostatic measurements *Math. Model. Numer. Anal.* **35** 595–605

[13] Brühl M, Hanke M and Vogelius M S 2003 A direct impedance tomography algorithm for locating small inhomogeneities *Numer. Math.* **93** 635–654

[14] Calderón A P 1980 On an inverse boundary value problem *Seminar on Numerical Analysis and its Application to Continuum Physics* ed W H Meyer and M A Raupp (Rio de Janeiro: Brasil. Math. Soc.) pp 65–73

[15] Cheney M, Isaacson D and Newell J C 1999 Electrical impedance tomography *SIAM Review* **41** 85–101

[16] Frühauf F, Gebauer B and Scherzer O 2007 Detecting interfaces in a parabolic-elliptic problem from surface measurements *SIAM J. Numer. Anal.* **45** 810–36

[17] Gebauer B 2006 The factorization method for real elliptic problems *Z. Anal. Anwend.* **25** 81–102

[18] Gebauer B, Hanke M, Kirsch A, Muniz W and Schneider C 2005 A sampling method for detecting buried objects using electromagnetic scattering *Inverse Problems* **21** 2035–2050.

[19] Griesmaier R 2007 An asymptotic factorization method for detecting small objects using electromagnetic scattering *submitted* preprint available online at http://numerik.mathematik.uni-mainz.de/ griesmaier/publications/asymptfact.pdf

[20] Hanke M and Brühl M 2003 Recent progress in electrical impedance tomography *Inverse Problems* **19** S65–S90.

[21] Hanke M and Schappel B 2007 The factorization method for electrical impedance tomography in the half space *accepted to SIAM J. Appl. Math.*

[22] Hyvönen N 2004 Complete electrode model of electrical impedance tomography: Approximation properties and characterization of inclusions *SIAM J. Appl. Math.* **64** 902–31

[23] Hyvönen N 2004 Characterizing inclusions in optical tomography *Inverse Problems* **20** 737–51

[24] Hyvönen N 2005 Application of a weaker formulation of the factorization method to the characterization of absorbing inclusions in optical tomography *Inverse Problems* **21** 1331–43

[25] Hyvönen N 2007 Application of the factorization method to the characterization of weak inclusions in electrical impedance tomography *Adv. in Appl. Math.* **39** 197–221

[26] Hyvönen N 2007 Locating transparent regions in optical absorption and scattering tomography *SIAM J. Appl. Math.* **67** 1101–1123

[27] Hyvönen N, Hakula H and Pursiainen S 2007 Numerical implementation of the factorization method within the complete electrode model of electrical impedance tomography *Inverse Probl. Imaging* **1** 299–317

[28] Ikehata M 2005 A new formulation of the probe method and related problems *Inverse Problems* **21** 413-26

[29] Kirsch A 1998 Characterization of the shape of a scattering obstacle using the spectral data of the far field operator *Inverse Problems* **14** 1489–512

[30] Kirsch A 2005 The factorization method for a class of inverse elliptic problems *Math. Nachr.* **278** 258-77

[31] Lechleiter A 2006 A regularization technique for the factorization method *Inverse Problems* **22** 1605–25

[32] Lechleiter A, Hyvönen N and Hakula H 2007 The factorization method applied to the complete electrode model of impedance tomography *submitted* preprint available online at `http://users.tkk.fi/u/nhyvonen/Papers/approximationCEM.pdf`

[33] Nachman A I 1988 Reconstructions from boundary measurements *Ann. of Math.* **128** 531–76

[34] Nachman A I 1996 Global uniqueness for a two-dimensional inverse boundary value problem *Ann. of Math.* **143** 71–96

[35] Nachman A I, Päivärinta L and Teirilä A 2007 On imaging obstacles inside inhomogeneous media *submitted* preprint available online at `http://www.rni.helsinki.fi/ ljp/files/NaPaTe2006.pdf`

[36] Nachman A I, Sylvester J and Uhlmann G 1988 An n-dimensional Borg-Levinson theorem *Comm. Math. Phys.* **115** 595–605

[37] Päivärinta L, Panchenko A and Uhlmann G 2003 Complex geometrical optics solutions for Lipschitz conductivities *Rev. Mat. Iberoamericana* **19** 57–72

[38] Siltanen S, Mueller J and Isaacson D 2000 An implementation of the reconstruction algorithm of A Nachman for the 2d inverse conductivity problem *Inverse Problems* **16** 681–99

[39] Somersalo E, Cheney M, Isaacson D and Isaacson E 1991 Layer stripping: a direct numerical method for impedance imaging *Inverse Problems* **7** 899–926

[40] Sylvester J 1990 An anisotropic inverse boundary value problem *Comm. Pure and Appl. Math.* **43** 201–32

[41] Sylvester J 1992 A convergent layer stripping algorithm for the radially symmetric impedance tomography problem *Comm. Partial Differential Equations* **17** 1955–94

[42] Sylvester J and Uhlmann G 1987 A global uniqueness theorem for an inverse boundary value problem *Ann. of Math.* **125** 153–69